**Biogeosciences
Discussions**

Characterization of turbulence and validation of fine-scale parametrization in the Mediterranean Sea during BOUM experiment

Y. Cuypers[1], P. Bouruet-Aubertot[1], C. Marec[2], and J.-L. Fuda[3]

[1]LOCEAN/IPSL, UMR7159, CNRS/UPMC/IRD, Paris, France
[2]TAKUVIK/UMI 3376, Université de Laval, Quebec, Canada
[3]Centre IRD de Nouméa, Nouvelle Calédonie

Correspondence to: Y. Cuypers (yannis.cuypers@locean-ipsl.upmc.fr)

BGD

8, 8961–8998, 2011

Turbulence and validation of fine-scale parametrization

Y. Cuypers et al.

Title Page

Abstract	Introduction
Conclusions	References
Tables	Figures

|◄ | ►|
◄ | ►

Back | Close

Full Screen / Esc

Printer-friendly Version

Interactive Discussion

Abstract

One main purpose of BOUM experiment was to give evidence of the possible impact of submesoscale dynamics on biogeochemical cycles. To this aim physical as well as biogeochemical data were collected along a zonal transect through the western and eastern basins. Along this transect 3 day fixed point stations were performed within anticyclonic eddies during which microstructure measurements were collected over the first 100 m. We focus here on the characterization of turbulent mixing induced by internal wave breaking. The analysis of microstructure measurements revealed a high level of turbulence in the seasonal pycnocline and a moderate level below with energy dissipation mean values of the order of 10^{-6} W kg^{-1} and 10^{-8} W kg^{-1}, respectively. Fine-scale parameterizations developed to mimic energy dissipation produced by internal wavebreaking were then tested against these direct measurements. Once validated a parameterization has been applied to infer energy dissipation and mixing over the whole data set, thus providing an overview over a latitudinal section of the Mediterranean sea. The results evidence a significant increase of dissipation at the top and base of eddies associated with strong near inertial waves. Vertical turbulent diffusivity is increased both in these regions and in the weakly stratified eddy core.

1 Introduction

During the last two decades increasing evidence has shown that dynamical vertical transport is a key factor controlling biogeochemical fluxes in the ocean, which need to be accurately quantified in order to represent adequately biogeochemical processes (Lewis, 1986; Denman and Gargett, 1983; Klein and Lapeyre, 2008). Two main processes account for vertical transport, upwelling resulting from divergent Ekman transport and turbulent mixing. Wind shear and convection are the main sources of turbulent mixing in the mixed layer, whereas breaking internal waves are responsible for most of mixing in the stratified ocean (Munk and Wunsch, 1998; Thorpe, 2004). An adequate

representation of these processes is of particular importance in oligotrophic regions where vertical transport generates an upward nutrient flux that directly sustains primary production in the depleted euphotic zone.

Among oligotrophic environments anticyclonic eddies have focused much attention since intrinsic processes locally enhance the vertical transport of nutrients in the euphotic layer (McGillicudy et al., 1999; Ledwell et al., 2008). In these regions upward doming of seasonal thermocline (and downward doming of the permanent thermocline) known as eddy pumping generates an uplift of nutrients enriched deeper layer, a process which can be enhanced from the secondary circulation generated by interactions between wind driven surface currents and eddy motion (Martin and Richards, 2001). Finally Ledwell et al. (2008) suggest that increased shear and mixing could result from near inertial wave trapping.

The Mediterranean sea is an oligotrophic environment affected by a significant mesoscale dynamics, and more specifically by anticyclonic eddies (Moutin et al., 2011). Regarding internal wave energy sources, the Mediterranean sea is also a specific region since energy mainly comes from the atmospheric forcing due to a weak tidal forcing. A main overall goal of the BOUM (Biogeochemistry from the Oligotrophic to the Ultraoligotrophic Mediterranean) is "the representation of the interactions between planktonic organisms and the cycle of biogenic elements, considering scales from single process to the whole Mediterranean Sea" (Moutin et al., 2011). A large part of the experiment was dedicated to the precise characterization of biogeochemical processes within three oligotrophic environments namely anticyclonic eddies (eddies A, B, C). During the experiment special effort was made to determine physical forcing and more specifically the vertical mixing which impacts most of biogeochemical processes studied and modeled within BOUM project (Bonnet et al., 2011; Mauriac et al., 2011).

To our knowledge estimates of vertical mixing from in situ measurements are very scarce in the Mediterranean sea. In a pioneering study, Woods and Wiley (1972) reported some estimation of mixing based on temperature microstructure measurements in the upper 100 m of Malta coastal waters. Very recently Gregg et al. (2011) performed

Title Page

Abstract | Introduction

Conclusions | References

Tables | Figures

◀ | ▶

◀ | ▶

Back | Close

Full Screen / Esc

Printer-friendly Version

Interactive Discussion

intensive microstructure measurements in the Cycladic plateau. However mixing processes reported in these studies are quite specific to the continental slope. In this paper we focus on the characterization of turbulent dissipation and mixing resulting from internal wave breaking within anticyclonic eddies in deeper areas of the Mediterranean sea. Turbulent processes are characterized from microstructure measurements in the upper 100 m which are used to validate a parametrization of energy dissipation based on fine scale internal wave shear and strain. This parametrization is then applied in order to characterize vertical mixing within eddies full depth range and the results are discussed in relationship with the specificity of internal wave dynamics in these environments. Finally vertical mixing is inferred from deep fine scale measurements all along the Mediterranean East-West transect thus providing a first insight of the impact of internal wave mixing at the basin scale.

2 Data and methods

The BOUM cruise took place in summer of 2008 (16 June–20 July) aboard the French Research Vessel l'Atalante. A 3000 km West-East transect was surveyed from the Rhône river mouth in the western part of the Mediterranean Sea to the Eratosthenes seamount in the eastern part (Fig. 1). Details of the measurements are provided in the introductory article by Moutin et al. (2011). We focus in this paper on turbulence and hydrographic measurements and their interpretation in the context of internal wave dynamics and mixing. Analysis of the eddy water masses and structure is given in the introductory article to this session by Moutin et al.

2.1 Hydrographic and current measurements

Conductivity Temperature Depth (CTD) measurements were performed for each using a SeaBird SBE911 instruments. Data were averaged over 1 m bin to filter spurious salinity peaks. Simultaneously currents were measured from a 300 kHz Lowered

broadband Acoustic Current Profiler (LADCP). LADCP data were processed using the Visbeck inversion method and provided current vertical profiles at 8 m resolution. Thirty CTD/LADCP profiles were collected along the BOUM transect down to the bottom during short duration (SD) station at an horizontal spatial resolution of $\simeq$100 km (see Fig. 1). In addition intensive measurements (every $\simeq$3 h over 3 days) were realized down to 500 m depth for each of the 3 long duration (LD) stations within anticyclonic eddies A, B and C (Fig. 1).

2.2 Dissipation measurements and K_z estimates

For each long duration station repeated profiles with a temperature gradient microstructure profiler, Self-Contained Autonomous Microstructure Profiler (SCAMP; Precision Measurements Engineering, www.PME.com), enabled estimates of energy dissipation rate (ϵ) and vertical diffusivity of temperature (K_z) to be made (e.g. Ruddick et al., 2000). SCAMP is limited to 100 m depth and operates at a slow optimal free fall velocity of 0.1–0.2 m s^{-1}. SCAMP was deployed only under calm weather conditions (low wind and swell) and between the CTD/LADCP profiles, therefore the total number of SCAMP profiles was limited to 21. Estimation of dissipation is based on Batchelor curve fitting of the temperature gradient spectrum (Ruddick et al., 2000). The maximum likelihood method of Ruddick et al. (2000) implemented in SCAMP software is used for the curve fitting. However we customize the algorithm by:

- including the improvement on the estimation of χ_T (the rate of destruction of temperature variance by molecular diffusion (°C s^{-1})^2) proposed by Steinbuck et al. (2009).

- switching to the least square fit method of Luketina et al. (2000) for very low χ_T. In this method the high wavenumber part of the spectrum dominated by noise is simply discarded rather than modeled and included as part of the fit, this appeared to be more efficient when noise variance was larger than χ_T.

The rate of cross-isopycnal turbulent mixing or diapycnal diffusivity K_{turb}, is commonly inferred from kinetic energy dissipation using the Osborn (1980) relationship:

$$K_{turb} = \Gamma \epsilon N^{-2} \tag{1}$$

where Γ is a mixing efficiency defined as the ratio between buoyancy flux and turbulent production and N is the buoyancy frequency. Following Osborn (1980) Γ is generally set to 0.2 which corresponds to the critical flux Richardson number $R_{crit} = 0.17$.

Recently in a numerical study, Shih et al. (2005) have shown that Osborn relationship could lead to overestimates of K_{turb} for turbulent flows characterized by turbulent intensity $\epsilon/\nu N^2$ larger than 100. They proposed a new parameterization for this regimes:

$$K_{turb} = 2\nu \left(\frac{\varepsilon}{\nu N^2} \right)^{\frac{1}{2}} \tag{2}$$

with $\nu = 1.9 \times 10^{-6} \, \text{m}^2 \, \text{s}^{-1}$.

Shih et al. also show that turbulent diffusion is inefficient below $\epsilon/\nu N^2$.

Therefore, following Shih et al. (2005) we apply Eq. (2) for $\epsilon/\nu N^2 > 100$ and Osborn relationship for $7 < \epsilon/\nu N^2 < 100$, whereas turbulent diffusion is considered null for $\epsilon/\nu N^2 < 7$. Note that a background molecular diffusion equal to the molecular diffusion of heat $\kappa_T = 1 \times 10^{-7} \, \text{m}^2 \, \text{s}^{-1}$ is always present, so that the final expression of diapycnal diffusivity including both turbulent and molecular diffusion reads $K_z = K_{turb} + \kappa_T$.

2.3 Fine scale parameterization

In the absence of microstructure measurements, energy dissipation is classically inferred from fine-scale parameterization which relates the characteristics of the internal wave field to energy dissipation. Basically, this relationship depends on the dynamics of the internal wave field that controls energy transfers toward small scales. Typically, as underlined by D'Asaro and Lien (2000), energy dissipation, ϵ, will scale like the

energy, E, of the internal wave field, when the energy level is "high", namely the characteristic timescale of energy transfers comparable or smaller than the period of the waves, whereas ϵ will scale like the energy squared, E^2, for a weakly non linear internal wave field. This latter class of parameterizations has been chosen here as the energy level of the IGW field is comparable to the reference energy level as detailed in the following.

Away from the boundaries, in the stratified ocean interior, the internal wave continuum is "reasonably" well represented by the GM79 spectrum (Garrett and Munk, 1979). Therefore parameterizations of energy dissipation, ϵ, based on this model of a weakly non linear internal field in which energy transfers are driven by resonant interactions, were developed (e.g. Henyey et al., 1986). In these parameterizations ϵ is formulated in terms of larger-scale parameters e.g. shear (vertical derivative of horizontal velocity) and/or strain (vertical derivative of isopycnal displacement) variances in the wavenumber range of internal waves. It is noteworthy to mention that these parameterizations are able to reproduce the observed levels of dissipation within a factor of two for conditions close to the GM79 model (Gregg et al., 1989). This is consistent with the main assumption, that of a weakly nonlinear internal wave field. We present here the popular incarnation of the original Henyey et al. (1986) parameterization proposed by Gregg (1989) (G89 hereafter):

$$\epsilon_{\text{IW}} = 1.8 \times 10^{-6} \left[f \cosh^{-1} \left(\frac{N_0}{f} \right) \right] \left(\frac{N^2}{N_0^2} \right) \left(\frac{S_{10}^4}{S_{\text{GM}}^4} \right) \tag{3}$$

where N_0 is the canonical GM buoyancy frequency, $S_{10\,\text{m}}$ is the shear inferred by differentiation over 10 m and S_{GM} the GM shear, with $S_{\text{GM}}^4 = 1.66 \times 10^{-10} \left(N^2/N_0^2 \right)^2$.

The main drawback of the G89 parameterization is its under-estimate of ϵ values in the ocean interior. There, as internal wave breaking comes into play as well, the higher frequency part of the wave field, for which strain dominates over shear, is not properly taken into account. Therefore, as in Kunze et al. (2006) and Gregg et al. (2003)

parameterizations, we introduced in G89 the additional factor:

$$h(R_\omega) = \frac{3(R_\omega + 1)}{2\sqrt{2}R_\omega\sqrt{R_\omega - 1}} \tag{4}$$

that takes into account the shear to strain ratio so that the the parameterization we proposed reads:

$$\epsilon_{param} = h(R_\omega)\epsilon_{IW} \tag{5}$$

However in the upper part of the water column $z > 25\,\mathrm{m}$ the shear is not properly measured by LADCP, therefore following Kunze et al. (2006) we estimate shear from strain as $S_{10}^2 = \langle R_\omega \rangle \left(\xi_z^2\right)_{10}$ where $(\xi_z)_{10}$ is the 10 m smoothed strain and $\langle R_\omega \rangle$ is the shear to strain ratio averaged over the lower part of the water column [20–100] m. Note that near the surface, for $z > 20\,\mathrm{m}$, the parameterization should be considered with caution due to the lack of shear measurements and to the strong deviation from GM79 conditions.

Finally we consider the effect of noise contamination in the computation of shear. Since noise velocity is white in wavenumber (Pinkel, 1985) the noise shear spectrum shows a k_z^2 wavenumber dependance and it may overcomes the physical shear signal for high wavenumber. This is particulary critical for deep measurements in low stratification environments and away from internal wave energy sources.

To turn around this problem low pass filtering of the signal is generally applied by either smoothing the LADCP signal using a running average (Alford and Gregg, 2001) or by truncating the shear spectra at some threshold wavenumber k_c above which the signal to noise ratio is not acceptable (Kunze et al., 2006). Here we determined the noise contamination by fitting the experimental shear spectra with a composite GM and k_z^2 shape. Both the energy level of noise and GM shaped spectrum are determined numerically from the fitting process. This allows to determine the wavenumber k_{noise} at which the noise spectra intersect the fitted GM shape and will strongly influence the measured shear. Figure 2a and b shows examples of mean shear spectra computed

in the upper ($z < 500$ m) and lower ($z > 500$ m) parts of the water columns of deep isolated LADCP profiles performed during short duration stations. Spectra in the upper 500 m are marginally affected by noise in contrast with spectra at larger depths for which we determined $k_{noise}/2\pi = 2 \times 10^{-2}$ cpm due to a much lower shear level. The LADCP profiles were low pass filtered using a numerical Finite Impulse response Filter (FIR) with cut off wavenumber $W \simeq 2\pi/k_{noise}$. Note that we used FIR filter rather than smoothing because it has a much sharper cut off. The filtered signal is then used to compute 10m shear in Eq. (3). Because some high wavenumber energy is removed from the experimental signal in this smoothing process we also smooth the stratification profile $N(z)$ in the computation of S_{GM}^4. This is roughly equivalent to the truncation of spectrum to k_c in the computation of experimental and GM shear variance in Kunze et al. (2006) parameterization. The underlying hypothesis in both cases is that the ratio of experimental to GM shear remains constant if both are low passed at the same wavenumber.

Figure 2c, d and e shows examples of mean shear spectra for the three long stations in eddies A, B and C. In this case the shear level is much above the noise level and noise is not an issue. As will be shown in the next section, this strong shear at stations A and C results from energetic near inertial waves in the eddies.

3 Observations-direct estimation of dissipation and validation of a fine scale parameterization

3.1 Stratification and dynamics at the three long duration stations

Three day stations were performed within three anticyclonic eddies with a three hour time sampling. This 3 h interval between profile allows both to characterize the background state- the low-pass stratification and currents, typically with filtering super-inertial oscillations, as well as the lower frequency band of the internal wave spectrum whose frequencies range within $[f, N]$ (Fig. 3). The mean surface stratification presents

a sharp pycnocline at ~ 15 m depth with values $\sim 3.10^{-3}$ rad s^{-1} which is typical of summer stratification in the Mediterranean Sea (Fig. 3g–i). Stratification next decreases and reaches minimum values in the core of the eddy. The best evidence is given by eddy C with a pycnostad over $[100, 350]$ m (Fig. 3g). This region of weaker stratification clearly defines the eddy core. Interestingly eddy C is fully sampled as opposed to eddy B for instance whose upper core extension is around 200 m and extends beyond 500 m depth (Fig. 3h). Eddy A in contrast displays a limited core within $[100, 200]$ m (Fig. 3i). The stratification presents two regions of strong gradients in the upper layer and at the base of the eddy which constitute robust barriers limiting vertical transfers of mass and nutrients. It is insightful to examine the dynamics in these regions as high frequency and/or small scale motions can provide a significant source of turbulence. As well the "mean" currents will provide information on the velocity field within the eddy and on the location of the Atalante with respect to the eddy center. Currents within eddies B and C are fairly constant along the vertical within the eddy core and evidence an anticyclonic rotation with a direction varying from NW to N and NE in eddy C and from NE to E and SE in eddy B. Within eddy A, typically around 150 m depth, the current rotates from SW to NE. Thus all profiles have been performed within the eddies at some distance from the center. We next examined temporal variability at higher frequencies. The dominance of the variability at the inertial frequency is visualized on the total current time- depth sections. Oscillations with sloping iso-phases indicate baroclinic waves. Interestingly these waves are localized at the top and base of the eddy (e.g. Fig. 3a and d) leading to significant shear in these well stratified regions.

In order to characterize the internal wave spectrum we have computed shear spectra (Fig. 4). Note that only part of the internal wave range is resolved by our 3 h sampling profiles since the maximum frequency of these waves, the buoyancy frequency N reaches values up to $o(0.1)$ rad s^{-1}, also the spectral resolution limited by the duration of the stations is of $\pm 0.15\,f$ for eddies B and C and of $\pm 0.13\,f$ for eddy A. A main peak around the inertial frequency is evidenced at stations A and C which is consistent with the time depth plots of the currents described in Fig. 3. The peak is largely shifted to

0.8 f for eddy A in the first 100 m which shows the existence of subinertial waves.

A peak around the semi diurnal tidal frequency is also evidenced below 100 m depth for these stations. The shape of the spectra corresponds fairly well to that predicted by the G79 model, the reference internal wave spectrum, although spectra at station B shows a flatter slope. The spectra level is below the GM level in the upper layer for the three stations (red curves in Fig. 4) and slightly above the GM level at the base of eddies C and A (black in Fig. 4) where a strong near inertial signal is observed. Overall the experimental spectra are comparable to GM and we shall test in the following section fine-scale parameterizations of energy dissipation that have been developed in this context of weakly nonlinear internal waves.

3.2 Dissipation measurements in the upper oceanic layer and validation of the fine scale parameterization

Figure 5 shows the first 50 m of individual profiles of dissipation recorded by the SCAMP during each long station A, B, C in the background fine scale strain internal wave field. The strongly intermittent nature of ϵ is clearly apparent on these profiles with values spanning several orders of magnitude $[10^{-11}, 5.10^{-6}]\,\mathrm{W\,kg^{-1}}$. A neat increase of dissipation $[10^{-8}, 5.10^{-6}]\,\mathrm{W\,kg^{-1}}$ is observed between 10 and 20 m depth. This depth range typically corresponds to variation of the pycnocline location under internal waves heaving for the three stations (Fig. 5) and it will be referred hereafter as the pycnocline region. The few values recorded above 10 m in the mixed layer were comparable to pycnocline values but were not considered further in the analysis because of the specific physics of the mixed layer (out of the scope of this paper) and possible ship contamination. Below 20 m depth low values of dissipation ($< 10^{-9}\,\mathrm{W\,kg^{-1}}$) are recorded with some sporadic events of high dissipations reaching $10^{-6}\,\mathrm{W\,kg^{-1}}$. On Fig. 5 the strain appears clearly related to internal waves induced isopycnal displacement, this is most obvious for station C where a strong near inertial signal is observed. As observed for dissipation the strain values are generally maximum in the pycnocline region which suggests internal wave strain importance in breaking processes as

already noted by several authors (Alford and Pinkel, 2000; Alford and Gregg, 2001; Alford, 2010). Still, no clear phase relationship is apparent between internal waves strain and dissipation here. A similar situation was observed by Alford (2010) for tidal and near inertial internal waves in the Mendocino escapement which suggests that dissipation results in this case from a cascading process as assumed by fine scale parameterization of dissipation (Sect. 2.3) rather than through direct breaking events of the dominant internal waves.

The question of the appropriate way to average such an intermittent variable as ϵ or K_z using experimentally limited number of samples has long been debated. Numerous observations of turbulent dissipation distribution in geophysical stratified flows are quite close to lognormal (Baker and Gibson, 1987; Gregg et al., 1993; Davis, 1996), which means that the logarithm of these variables is approximately normally distributed. Baker and Gibson (1987) argue that Lognormal distribution of dissipation observed in oceanic environments can indeed be explained within the framework of homogeneous isotropic turbulence (Kolmogoroff, 1967) multiplicative cascades for homogeneous isotropic turbulence. Therefore Baker and Gibson (1987) suggest to use Maximum Likelihood Estimates of the mean dissipation expected for a lognormal distribution which reads:

$$\langle \epsilon \rangle_{\text{MLE}} = \exp\left(\mu + \frac{1}{2}\sigma^2\right) \tag{6}$$

where $\mu = \langle \log(\epsilon) \rangle$ and $\sigma = \text{std}(\log(\epsilon))$.

Davis (1996) and Gregg et al. (1993) criticize Baker and Gibson (1987) approach, considering that oceanic observations of turbulence are far from fulfilling isotropic and homogeneous turbulence assumptions and can only be approximately lognormal. Given these caveats, Davis (1996) suggests that a simple arithmetic mean is the most reliable estimate. However as outlined by Gargett (1999) arithmetic mean will strongly be affected by infrequent outliers. Sometimes a geometric mean (equivalent to the exponential of the mean of the logarithm of dissipation) is computed in order to reduce the dispersion of dissipation data (Gargett, 1999; Smyth et al., 1997).

The statistical distribution of dissipation for all data and each station separately is represented as a Probability Density Function (PDF) of ϵ in Fig. 6. Regions between 10 and 20 m depth referred to hereafter as the pycnocline region which corresponds to the depth range of variation of the seasonal pycnocline under internal waves heaving (Fig. 5) and below 20 m depth were distinguished. The PDF were truncated below 10^{-11} W kg^{-1} and above 10^{-5} W kg^{-1} which represents the upper and lower bound of the SCAMP resolution. A lognormal distribution truncated at these resolution bounds was fitted to each PDF by Maximum Likelihood. An estimate of the mean was then obtained from the fit by Eq. (6). This MLE of the mean as well as the arithmetic and geometric mean and their confidence interval are given in Table 1.

For all stations, the PDF show two dynamical regions, for data in the pycnocline region the most probable value (mode value) is $\sim 2.10^{-7}$ W kg^{-1} which characterizes highly dissipative processes, whereas it is close to a fairly low dissipation value of 10^{-10} W kg^{-1} below. Below the pycnocline, the PDF is rather close to a lognormal distribution for station C, but is more skewed and spiky for stations B and A, which may results partially from lack of convergence of experimental PDF. The lack of sampling in the limited pycnocline region does not allow to state whether distributions of dissipation are lognormal there.

All in all the arithmetic mean and MLE fit mean are quite close below the pycnocline for all stations with values $\sim 10^{-8}$ W kg^{-1} (Table 1). These mean values are almost two orders of magnitude larger than the most probable value which illustrates the large intermittency of the data. The geometric mean largely underestimates the dissipation with a value $\sim 10^{-10}$ W kg^{-1} which is closer to the mode value. In the pycnocline region, the mean dissipation is almost two orders of magnitude higher. Arithmetic mean of dissipation is lower at station C $\sim 10^{-7}$ W kg^{-1} than at stations B and A $\sim 10^{-6}$ W kg^{-1}.

Figure 7 shows PDF of K_z truncated in the range $[10^{-7}, 10^{-3}]$ m^2 s^{-1}. The PDF also shows two dynamical regions, a flat distribution with a mode value of $K_z \sim 3.10^{-7}$ m^2 s^{-1} is observed below 20 m and a highly spiked distribution with mode value of $\sim 5.10^{-5}$ m^2 s^{-1} is found in the pycnocline region. Below the pycnocline some

reasonable agreement is found between the MLE lognormal fit and K_z distribution for station C, elsewhere no lognormal behavior could be evidenced. The arithmetic mean of K_z below the pycnocline is $\sim 1.10^{-5}\,\mathrm{m^2\,s^{-1}}$ for all stations, whereas MLE estimate at station C reaches $1.9 \times 10^{-5}\,\mathrm{m^2\,s^{-1}}$. In the pycnocline region depth arithmetic mean K_z values are higher by a factor ~ 5. Geometric means largely underestimate K_z by nearly 2 order of magnitudes below the pycnocline, but agrees within a factor of 3 above 20 m. The increase of K_z in the pycnocline region observed here is unusual because the larger stratification generally prevents the increase of mixing. It results here from high mean dissipation reaching $\sim 6.6 \times 10^{-6}\,\mathrm{W\,kg^{-1}}$ in the pycnocline region and its dramatic decrease below the seasonal pycnocline.

From this analysis we also find that MLE of ϵ from a lognormal distribution when applicable and arithmetic mean gave similar results, therefore following Davis (1996) advise we will simply consider arithmetic mean in the following.

We next look at the ensemble averaged vertical profiles of ϵ and compare them with the parameterization proposed in Sect. 2.3. In order to reduce dispersion of ϵ and K_z values and to allow better comparison with parameterization based on 10 m scale shear, ϵ and K_z profiles were first smoothed using a 10 m running average. Depth average profiles of ϵ and K_z were then computed (Fig. 8 and 9). When averaged over all profiles, dissipation decreases from high values of $10^{-6}\,\mathrm{W\,kg^{-1}}$ to moderate values of $10^{-8}\,\mathrm{W\,kg^{-1}}$ between 10 m and 40 m depth. Below dissipation remains around a pretty constant value of $10^{-8}\,\mathrm{W\,kg^{-1}}$. This dissipation level is comparable with the GM reference level ϵ_{GM} that mostly falls within the 95 % confidence interval below 40 m, but overcomes ϵ_{GM} from more than one order of magnitude in the pycnocline [10 m, 20 m].

Station average profiles show larger variability at depth that likely results from the lack of statistics as illustrated by the largest confidence intervals. Station B however shows a neat low dissipation $\simeq 10^{-10}\,\mathrm{W\,kg^{-1}}$ below ϵ_{GM} between 50 and 70 m depth which is one order of magnitude smaller than GM level.

The parameterized dissipation e_{param} shows a fairly good agreement with SCAMP measurements. When the average of the whole set of profiles is considered $\langle e_{param} \rangle$ falls within the 95 % interval of SCAMP measurements over 85 % of the profile depth range. The agreement is also good when average is performed independently for each station, the overall shape of the SCAMP average profile is well reproduced by the parameterization, notably the decrease of dissipation in the first thirty meters and the lower dissipation at station B around 55 m depth. However large discrepancies exceeding one order of magnitude are punctually observed, but those occur mostly for stations B and A where a very small number of profiles is available.

K_z depth averaged profiles are shown in Fig. 9 the whole profile set average shows decreasing values from $5.10^{-5}\,\mathrm{m^2\,s^{-1}}$ to $10^{-6}\,\mathrm{m^2\,s^{-1}}$ between 10 m and 40 m depth and then slowly increasing values up to to $5.10^{-5}\,\mathrm{m^2\,s^{-1}}$ at 95 m depth. Top and bottom values are significantly higher than the nearly constant GM value of $5.10^{-6}\,\mathrm{m^2\,s^{-1}}$, whereas the local minimum at 40 m depth is lower. Station average evolve in the same range with a noticeable minimum of $\simeq 10^{-6}\,\mathrm{m^2\,s^{-1}}$ for station B between 45 and 70 m depth. For station A, K_z remains highly variable in the range $10^{-6}\,\mathrm{m^2\,s^{-1}}$ $5.10^{-5}\,\mathrm{m^2\,s^{-1}}$ due to the lack of statistics.

The proportion of the different diffusion regimes found according to Shih et al. (2005) classification (Sect. 2.2) is also shown in Fig. 8 and 9. Intermediate and strong turbulence regime dominates in the pycnocline, whereas molecular diffusion dominates below 25 m depth, the minimum of turbulent diffusion around 40 corresponds to region where molecular diffusion regime is found for 80 % of the samples.

Overall average of parameterized K_z are close to experimental values and falls within the experimental confidence interval over 90 % of the profile depth range. However the local minima around 40 m depth is not reproduced.

4   Dissipation and turbulent mixing inferred from fine-scale parameterization

The modified G89 parameterization, validated by SCAMP measurements, was applied to the full dataset. Time depth plots of ϵ and K_z are displayed for the three LD stations in Fig. 10 whereas the stations averaged profiles are shown in Fig. 11. The domain of variation is large within $[10^{-12}, 10^{-5}]\,\mathrm{W\,kg^{-1}}$ for ϵ and within $[10^{-7}, 10^{-3}]\,\mathrm{m^2\,s^{-1}}$ for K_z. The eddy core is characterized by weak values of dissipation, $o(10^{-10}\,\mathrm{W\,kg^{-1}})$, as shown in Fig. 10a to c, with the most striking evidence for eddy C which has the largest vertical extension. In contrast the highest values are observed at the base (eddy C and eddy A) and at the top of the eddies (C, B and A). This increase in dissipation can be related to the high shear values at the boundaries of the eddies that results both from the mean current profile and from strong near-inertial internal waves for eddies A and C. This impact of near inertial internal waves on dissipation is best evidenced in eddy C within [400–500] m depth and between 160 m and 300 m for eddy A. The spatial distribution of vertical diffusivities differ from that of ϵ since stratification comes into play: regions of the weakest stratification, typically the eddy cores (see eddies C and B), are characterized by relatively large values of K_z, $\simeq 10^{-4}\,\mathrm{m^2\,s^{-1}}$ locally, which are of the same order as those at the base of the eddy associated with waves.

The parameterization was also applied to the deep stations performed all along the BOUM transect thus providing a snap shot of dissipation and mixing (Fig. 12). Figure 12 also shows the evolution of shear and stratification along the transect. The signature of eddies A, B and C is evidenced by a depression of upper isopycnes as well as local region of minimum stratification in Fig. 12. Same feature is observed for the Ierapetra anticyclonic eddy in the south of Crete that was also sampled during a SD station.

Highest shear and dissipation values are found in the upper 500 m and up to 1500 m above the bottom while these variables are generally minimum in a region between 500 m and 1500 m depth. As for LD stations data high shear and dissipation are found at the base of eddies A and C (at $x = 433$, and $3130\,\mathrm{km}$), but some enhancement

Title Page

Abstract | Introduction

Conclusions | References

Tables | Figures

◄ | ►►

◄ | ►

Back | Close

Full Screen / Esc

is also evidenced around 600 m at the base of eddy B ($x = 1810$ km) which was not sampled by LD stations profiles. Similarly high shear and dissipation are found at the base of Ierapetra eddy ($x = 2478$ km, $z \simeq 170$ m). Another noticeable feature is the large enhancement of shear and dissipation at $x = 1478$ km in the strait of Sicily which is likely associated with topographic effect (internal tides and/or bottom shear).

K_z values rapidly increase with decreasing stratification, therefore the dominant trend is an increase with depth. At large depth close to the bottom slight enhancement of dissipation and very weak stratification combine to give the largest vertical turbulent diffusion reaching locally 10^{-3} m^2 s^{-1}.

5 Discussion

Lacking dedicated physical measurements of dissipation previous biogeochemistry oriented studies have considered rough estimates of dissipation as a constant value in the computation of vertical turbulent diffusion ignoring large variations resulting from the fine scale internal wave field (Moutin and Raimbault, 2002; Copin-Montegut, 2000). For instance Moutin and Raimbault (2002) considered a constant value of $\epsilon = 7.10^{-10}$ W kg^{-1} to estimate vertical diffusion and nutrients fluxes in the upper 100 m during the MINOS cruise along the Mediterranean Sea. This value corresponds to a GM level dissipation at a reference stratification $N_0 = 3$ cph at the top of the pycnocline in G89 parameterization. As noted by Moutin and Raimbault (2002) this value is nearly two orders of magnitude smaller than the constant value of 5×10^{-8} W kg^{-1} (derived form Denman and Gargett, 1983) considered by Copin-Montegut (2000) in North Western Mediterranean sea. Clearly fluxes estimations could drastically change depending on the chosen value for ϵ. The slightly adapted G89 parametrization we propose here will improve significantly estimation of mixing compared to these previous rough estimates.

Parameterized ϵ estimated here from SD LADCP/CTD profiles along the Mediterranean transect show a mean value $\simeq 1.5 \times 10^{-9}$ W kg^{-1} below the seasonal pycnocline

and 100 m depth which is slightly higher than Moutin and Raimbault (2002) value. Higher dissipation was however found within eddies where the average dissipation directly estimated from SCAMP measurements and parameterization reaches $\simeq 8.5 \times 10^{-9}\,\mathrm{W\,kg^{-1}}$ for the same depth range which is in between Copin-Montegut

5 (2000) and Moutin and Raimbault (2002) values. The increase of ϵ and derived K_z in eddies is even more obvious in region of high near inertial shear at the base of eddies A and C.

These results suggest a strong influence of anticyclonic eddies on near inertial waves dynamics and mixing. Indeed anticyclonic eddies induce a negative background vor-

10 ticity which influence inertial waves propagation. L. Prieur (personal communication) estimated eddies vorticity from an analysis of drifting mooring trajectories deployed during BOUM (data not shown here). He finds the strongest negative vorticity for eddy A which reaches $\zeta = -0.397f$, a slightly weaker vorticity for eddy C reaching $\zeta = -0.32f$ and a weaker vorticity of $-0.297f$ for eddy B. Negative background vorticity can result

15 in a trapping of near inertial waves and explain enhanced near inertial shear. Indeed as shown by the theoretical work of Kunze (1985) anticyclonic mesoscale vorticity ζ induces locally a slight decrease of the effective inertial frequency $f_{\text{eff}} = f + \zeta/2$, therefore near inertial waves which evolve in the frequency band $[f_{\text{eff}}, N]$ will encounter their turning points when propagating away from anticyclonic eddy centers (Bouruet-Aubertot

20 et al., 2005) and remained trapped in the eddy core. Numerical studies by Lee and Niiler (1998), have also shown some increase of near inertial shear resulting from the interaction of near inertial waves with frontal structures or eddies validating partially the mechanism proposed by Kunze (1985). Evidence of a subinertial peak is indeed found at $f_{\text{eff}} = 0.8f$ at station A in the first 100 m which is in agreement with a shift

25 of 0.5ζ. Although spectral analysis (Sect. 3.1) did not reveal a subinertial peak at stations B and C, slightly subinertial waves can not be ruled out for theses stations because of the coarse resolution of $\pm 0.15\,f$ and the weaker vorticity of these eddies. The spectacular increase of near inertial shear at the base of eddy A and C may result more particulary from the vertical trapping of near inertial waves specific to baroclinic

anticyclonic structures where vorticity and thus f_{eff} increases with depth (Kunze, 1985). This mechanism was experimentally observed in a warm core ring (anticyclonic) of the Gulf Stream (Kunze, 1995) together with a (10–100) increase of dissipation. Another possible mechanism is a radiation of near inertial waves from a baroclinic adjustment of the eddy. Further work is needed to get insight of this near inertial waves generation at the eddy base.

Vertical mixing estimate within eddies in BOUM can be compared with previous studies of mixing within eddies based on tracer release experiments. Such tracer experiments integrates vertical transport processes over a large spatial scale (typically a region below the seasonal pycnocline and above 100 m depth) and temporal scale (a few days). Regarding turbulent mixing it is an advantage because it avoids problems related to the under sampling of highly intermittent turbulent mixing processes, but it also precludes a dynamical characterization of intermittent internal wave breaking as done here. Kim et al. (2005) and Ledwell et al. (2008) found $K_z \simeq 3.10^{-5}\,\text{m}^2\,\text{s}^{-1}$ between the base of a shallow seasonal mixed layer and 100 m depth in North Atlantic anticyclonic eddies (46° N) and in the Sargasso sea (31° N) respectively. Whereas one order of magnitude higher values were found by Law et al. (2001) also in a North Atlantic anticyclonic eddy (59° N). In BOUM experiment the overall averaged K_z found within eddies A, B and C pycnocline base and 100 m depth is $\simeq 10^{-5}\,\text{m}^2\,\text{s}^{-1}$ which is two times the GM value but is still three times smaller than Kim et al. (2005) and Ledwell et al. (2008) estimates. However wind forcing was pretty weak during BOUM, whereas all the experiments cited above were affected by the passage of storms (Law et al., 2001; Ledwell et al., 2008) or strong wind gusts (Kim et al., 2005) that likely increased internal waves energy and induced dissipation. It should also be noted that Greenan (2008) provides smaller K_z estimates than Ledwell et al. (2008) from Gregg-Henyey (1989) parameterization of dissipation for the same experiment (EDDIES).

Full Screen / Esc

Printer-friendly Version

Interactive Discussion

6 Concluding remarks

In this study we proposed a slightly adapted G89 parameterization for dissipation which was validated against microstructure estimates in the first 100 m of the water column. The energy sources for internal waves are weak in summer in the Mediterranean sea, therefore the background parameterized dissipation found from deep SD stations along the transect is relatively weak below the base of the seasonal pycnocline and away from the bottom leading to weak vertical turbulent diffusion $\simeq 10^{-5}\,\mathrm{m^2\,s^{-1}}$ in these regions. A contrasting situation was found in eddies where large near inertial at eddy top and bottom is associated with dissipation exceeding the canonical GM level. Turbulent diffusion increased in these regions of high shear and dissipation but also within the eddy core because of a much weaker stratification within this homogenous mass of water. The spectacular increase of near inertial shear found in eddies likely result from trapping or channeling of near inertial energy input at the surface, a mechanism highlighted in several numerical and experimental studies (Kunze, 1985, 1995; Lee and Niiler, 1998; Bouruet Aubertot et al., 2005).

Further studies implicating BOUM experimental results and numerical model will allow to characterize thoroughly the impact of mesoscale eddies on biogeochemical processes. Statistical distribution of vertical diffusion may notably be used to reproduce the impact of the strong intermittency of turbulence in one-dimensional biogeochemical model already available (Mauriac et al., 2011). However, regarding the impact on nutrients fluxes, Bonnet et al. (2011) have shown that vertical dinitrogen turbulent fluxes determined from K_z values obtained in eddies still balance only a small fraction of the nitrogen fixation fluxes resulting from primary production suggesting a main contribution from atmospheric deposition. Vertical advection was not considered in this study and may as well provide significant vertical transport of nutrients as suggested in previous studies (Ledwell, 2008).

References

Alford, M. H.: Internal swell generation: The spatial distribution of energy flux from the wind to mixed-layer near-inertial motions, J. Phys. Oceanogr., 31, 2359–2368, 2001.

Alford, M. H.: Sustained, full-water-column observations of internal waves and mixing near Mendocino Escarpment, J. Phys. Oceanogr., 40, 2643–2660, 2010.

Alford, M. H. and Pinkel, R.: Observations of overturning in the thermocline: The context of ocean mixing, J. Phys. Oceanogr., 30, 805–832, 2000.

Baker, M. A. and Gibson, C. H.: Sampling turbulence in the stratified ocean: statistical consequences of strong intermittency, J. Phys. Oceanogr., 17, 1817–1836, 1987.

Bonnet, S., Grosso, O., and Moutin, T.: Planktonic dinitrogen fixation along a longitudinal gradient across the Mediterranean Sea during the stratified period (BOUM cruise), Biogeosciences, 8, 2257–2267, doi:10.5194/bg-8-2257-2011, 2011.

Bouruet-Aubertot, P., Mercier, H., Gaillard, F., and Lherminier, P.: Evidence of strong inertia-gravity wave activity during the POMME experiment, J. Geophys. Res., 110, C07S06, doi:10.1029/2004JC002747, 2005.

Copin-Montegut, C.: Consumption and production on scales of a few days of inorganic carbon, nitrate and oxygen by the planktonic community: results of continuous measurements at the

Title Page

Abstract | Introduction

Conclusions | References

Tables | Figures

Back | Close

Full Screen / Esc

Printer-friendly Version

Interactive Discussion

DYFAMED Station in the northwestern Mediterranean Sea (May 1995), Deep-Sea Res. I, 47, 447–477, 2000.

D'Asaro, E. A. and Lien, R.: The Wave-Turbulence Transition for Stratified Flows, J. Phys. Oceanogr., 30, 1669–1678, 2000.

Davis, R. E.: Sampling turbulent dissipation, J. Phys. Oceanogr., 26, 341–358, 1996.

Denman, K. L. and Gargett, A. E.: Time and space scales of vertical mixing and advection of phtoplankton in the upper ocean, Limnol. Oceanogr., 28, 801–815, 1983.

Gargett, A. E.: Velcro Measurement of Turbulence Kinetic Energy Dissipation Rate ϵ, J. Atmos. Oceanic Technol., 16, 1973–1993, 1999.

Garrett, C. and Munk, W.: Internal waves in the ocean, Annu. Rev. Fluid Mech., 11, 339–369, 1979.

Gregg, M. C.: Scaling turbulent dissipation in the thermocline, J. Geophys. Res., 94, 9686–9698, 1989.

Gregg, M. C., Seim, H. E., and Percival D. B.: Statistics of shear and turbulent dissipation profiles in random internal wave fields, J. Phys. Oceanogr., 23, 1777–1799, 1993.

Gregg, M. C., Sandford, T. B., and Winkel, D. P.: Reduced mixing from the breaking of internal waves in equatorial waters, Nature, 422, 513–515, 2003.

Gregg, M. C., Alford, M. H., Kontoyiannis, H., Zervakis, V., and Winkel, D.: Mixing over the steep side of the Cycladic Plateau in the Aegean Sea, J. Marine Sys., accepted, doi:10.1016/j.jmarsys.2011.07.009, 2011.

Henyey, F. S., Wright, J., and Flatte, S. M.: Energy and action flow through the internal wave field, J. Geophys. Res., 91, 8487–8495, 1986.

Kim, D., Kitack, L., Sung-Deuk, C., Hee-Sook, K., Jia-Zhong, Z., and Yoon-Seok, C.: Determination of diapycnal diffusion rates in the upper thermocline in the North Atlantic Ocean using sulfur hexafluoride, J. Geophys. Res., 110, C10010, doi:10.1029/2004JC002835, 2005.

Klein, P. and Lapeyre, G.: The Oceanic Vertical Pump Induced by Mesoscale and Submesoscale Turbulence, Annu. Rev. Mar. Sci., 1, 351–375, 2009.

Kunze, E.: Near-inertial wave propagation in geostrophic shear, J. Phys. Oceanogr., 14, 544–565, 1985.

Kunze, E.: The energy balance in a warm-core ring's near-inertial critical layer, J. Phys. Oceanogr., 25, 942–957, 1995.

Kunze, E., Firing, E., Hummon, J. M., Chereskin, T. K., and Thurnherr, A. M.: Global abyssal mixin inferred from Lowered ADCP shear and CTD strain profiles, J. Phys Oceanogr., 36(8),

1553–1576, 2006.

Law, C. S., Martin, A. P., Liddicoat, M. I., Watson, A. J., Richards, K. J., and Woodward, E. M. S.: A Lagrangian SF6 tracer study of anticyclonic eddy in the North Atlantic: Patch evolution, vertical mixing and nutrient supply to the mixed layer, Deep Sea Res., Part II, 48, 705–724, 2001.

Ledwell, J. R., McGillicuddy, D. J., and Anderson, L. A.: Nutrient flux into an intense deep chlorophyll layer in a mode-water eddy, Deep Sea Res. II, 55, 1139–1160, 2008.

Lee, D. K. and Niiler, P. P.: The inertial chimney: The near-inertial energy drainage from the ocean surface to the deep layer, J. Geophys. Res., 103(C4), 7579–7591, 1998.

Lewis, M. R., Harrison, W. G., Oakey, N. S., Hebert, D., and Platt, T.: Vertical nitrate flux in the Oligotrophic Ocean, Science, 234, 870–873, 1986.

Luketina, D. A. and Imberger, J.: Determining turbulent kinetic energy dissipation from Batchelor curve fitting, J. Atmos. Oceanic Technol., 18, 100–113, 2001.

Martin, A. P. and Richards, K. J.: Mechanisms for vertical nutrient transport within a North Atlantic mesoscale eddy, Deep-Sea Res. II, 48, 757–773, 2001.

Mauriac, R., Moutin, T., and Baklouti, M.: Accumulation of DOC in Low Phosphate Low Chlorophyll (LPLC) area: is it related to higher production under high N:P ratio?, Biogeosciences, 8, 933–950, doi:10.5194/bg-8-933-2011, 2011.

Mc Comas, C. H. and Muller, P.: The Dynamic Balance of Internal Waves, J. Phys. Oceanogr., 11, 970–986, 1981.

McGillicuddy, D. J., Johnson, R., Siegel, D. A., Michaels, A. F., Bates, N. R., and Knap, A. H.: Mesoscale variations of biogeochemical properties in the Sargasso Sea, J. Geophys. Res., 104, 13381–13394, 1999.

Moutin, T. and Raimbault, P.: Primary production, carbon export and nutrients availability in western and eastern Mediterranean Sea in early summer 1996 (MINOS cruise), J. Marine Sys., 33–34, 273–288, 2002.

Moutin, T., Van Wambeke, F., and Prieur, L.: The Biogeochemistry from the Oligotrophic to the Ultraoligotrophic Mediterranean (BOUM) experiment, Biogeosciences Discuss., 8, 8091–8160, doi:10.5194/bgd-8-8091-2011, 2011.

Munk, W. and Wunsh, C.: Abyssal recipes II: Energetics of tidal and wind mixing, Deep Sea Res. II, 45, 1977–2010, 1998.

Osborn, T. R.: Estimates of the local rate of vertical diffusion from dissipation measurements, J. Phys. Oceanogr., 10, 83–89, 1980.

Title Page

Abstract | Introduction

Conclusions | References

Tables | Figures

◄◄ | ►►

◄ | ►

Back | Close

Full Screen / Esc

Printer-friendly Version

Interactive Discussion

Pinkel, R.: A wavenumber frequency spectrum of upper ocean shear, J. Phys. Oceanogr., 15, 1453–1569, 1985.

Ruddick, B., Anis, A., and Thompson, K.: Maximum Likelihood Spectral Fitting: The Batchelor Spectrum, J. Atmos. Oceanic Technol., 17, 1541–1554, 2000.

5 Shih, L. H., Koseff, J. R., Ivey, G. N., and Ferziger, J.: Parameterization of turbulent fluxes and scales using homogeneous sheared stably stratified turbulence simulations, J. Fluid Mech., 525, 193–214, 2005.

Smyth, W. D., Poliakov, P. O., and Moum, J. N.: Decay of Turbulence in the Upper Ocean following Sudden Isolation from Surface Forcing, J. Phys. Oceanogr., 27, 810–822, 1997.

10 Steinbuck, J. V., Stacey, M. T., and Monismith, S. G.: An Evaluation of χ_T Estimation Techniques: Implications for Batchelor Fitting and ϵ, J. Atmos. Oceanic Technol., 26, 1652–1662, 2009.

Thorpe, S. A.: Recent developments in the study of ocean turbulence, Annu. Rev. Earth Planet. Sci., 32, 91–109, 2004.

15 Woods, J. D. and Wiley, R. L.: Billow turbulence and ocean microstructure, Deep Sea Res., 19, 87–121, 1972.

Title Page

Abstract   Introduction

Conclusions   References

Tables   Figures

◀│   ▶│

◀   ▶

Back   Close

Full Screen / Esc

Printer-friendly Version

Interactive Discussion

Table 1. Mean SCAMP e estimations ($\mathrm{W\,kg^{-1}}$) from various methods, arithmetic mean, MLE of the lognormal distribution mean, geometric mean.

Range	Eddy	e_{arith}	e_{MLE}	e_{geom}
[20–100] m	All	8.5 [6.0 10.] (× 1e−9)	7.0 [3.1 16.] (× 1e−9)	1.5 [1.3 1.7] (× 1e−10)
	C	6.0 [3.2 8.0] (× 1e−9)	5.9 [2.3 13.] (× 1e−9)	1.5 [1.3 1.8] (× 1e−10)
	B	13. [7.0 19.] (× 1e−9)	16. [2. 170] (× 1e−9)	1.7 [1.3 2.1] (× 1e−10)
	A	8.0 [3.6 12.] (× 1e−9)	4.0 [0.4 50.] (× 1e−9)	1.3 [1.0 1.8] (× 1e−10)
[10–20] m	All	6.6 [4.4 9.0] (× 1e−7)	9.5 [2.4 4.4] (× 1e−6)	4.3 [3.0 6.0] (× 1e−8)
	C	1.9 [1.4 2.3] (× 1e−7)	1.6 [0.4 6.9] (× 1e−6)	2.3 [1.7 6.6] (× 1e−8)
	B	12. [7.0 18.] (× 1e−7)	NA	13. [8.0 25.] (× 1e−8)
	A	8.0 [3.5 13.] (× 1e−7)	NA	3.0 [1.7 6.6] (× 1e−8)

Table 2. Mean K_z estimations ($m^2\,s^{-1}$) from various methods, arithmetic mean, MLE of the lognormal distribution mean, geometric mean.

Range	Eddy	$K_{z,arith}$	$K_{z,MLE}$	$K_{z,geom}$
[20–100] m	All	1.3 [1.1 1.5] (× 1e−5)	NA	7.3 [6.6 6.4] (× 1e−7)
	C	1.0 [0.8 1.3] (× 1e−5)	1.9 [0.6 6.0] (× 1e−5)	9.2 [8.3 9.3] (× 1e−7)
	B	1.7 [1.3 2.2] (× 1e−5)	NA	6.2 [5.0 5.4](× 1e−7)
	A	1.5 [0.9 1.9] (× 1e−5)	NA	3.5 [2.9 5.0] (× 1e−7)
[10–20] m	All	4.7 [4.0 5.5] (× 1e−5)	NA	1.0 [0.6 1.3] (× 1e−5)
	C	3.0 [2.6 3.6] (× 1e−5)	7.0 [3.6 14.] (× 1e−5)	0.8 [0.3 1.0] (× 1e−5)
	B	6.9 [5.0 8.6] (× 1e−5)	NA	2.1 [1.2 3.0] (× 1e−5)
	A	5.2 [3.3 7.7] (× 1e−5)	NA	0.7 [0.4 1.3] (× 1e−5)
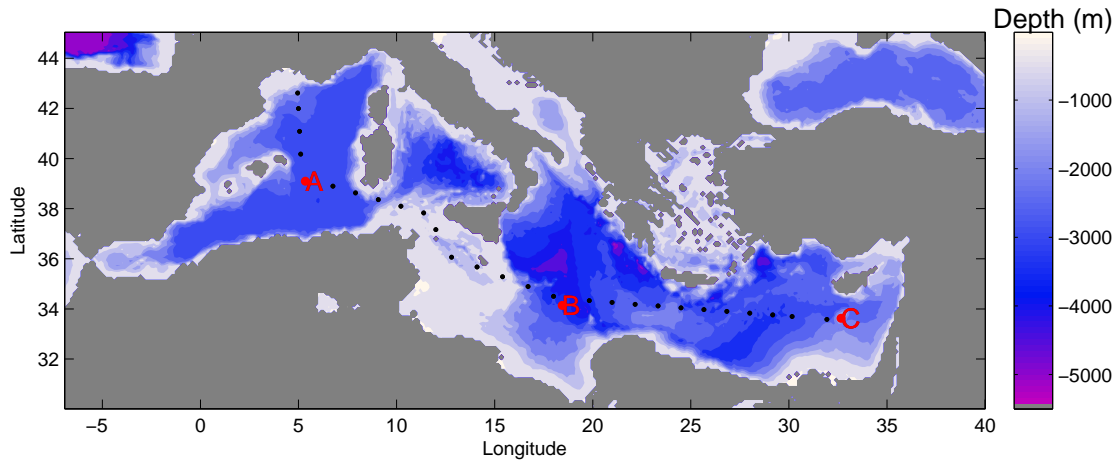
Fig. 1. Bathymetric map of the Mediterranean sea, short duration stations (SD) profiles are marked by black dots, long duration LD stations (A, B, C) at the eddy centers are marked by red dots.
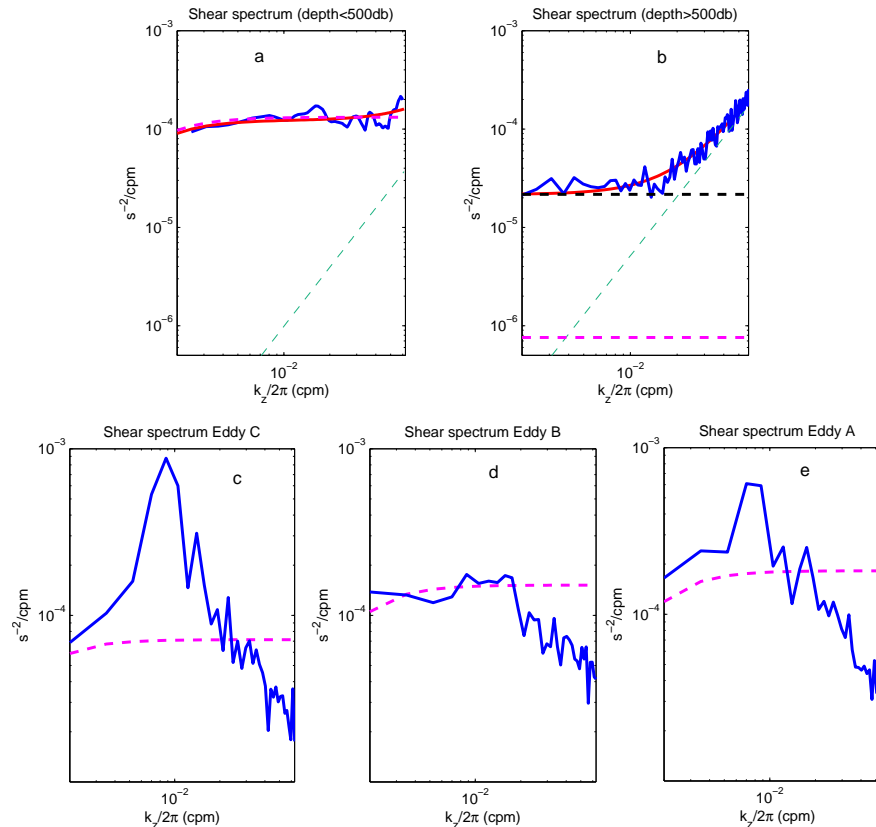
Fig. 2. Upper row: wavenumber vertical shear spectrum for deep SD stations LADCP profiles **(a)** $0 < z < 500$ m; **(b)** $z > 500$ m and lower row ensemble averaged wavenumber vertical shear spectra for LD stations LADCP profiles at **(c)** eddy C; **(d)** eddy B and **(e)** eddy A. The blue line, magenta dashed line, black dashed line, cyan dashed line and the red line represent respectively raw data shear spectrum, the GM level shear spectrum, the fitted GM shear spectrum, the noise fitted spectrum, and the composite of noise and GM fitted spectra.

Full Screen / Esc

Printer-friendly Version

Interactive Discussion
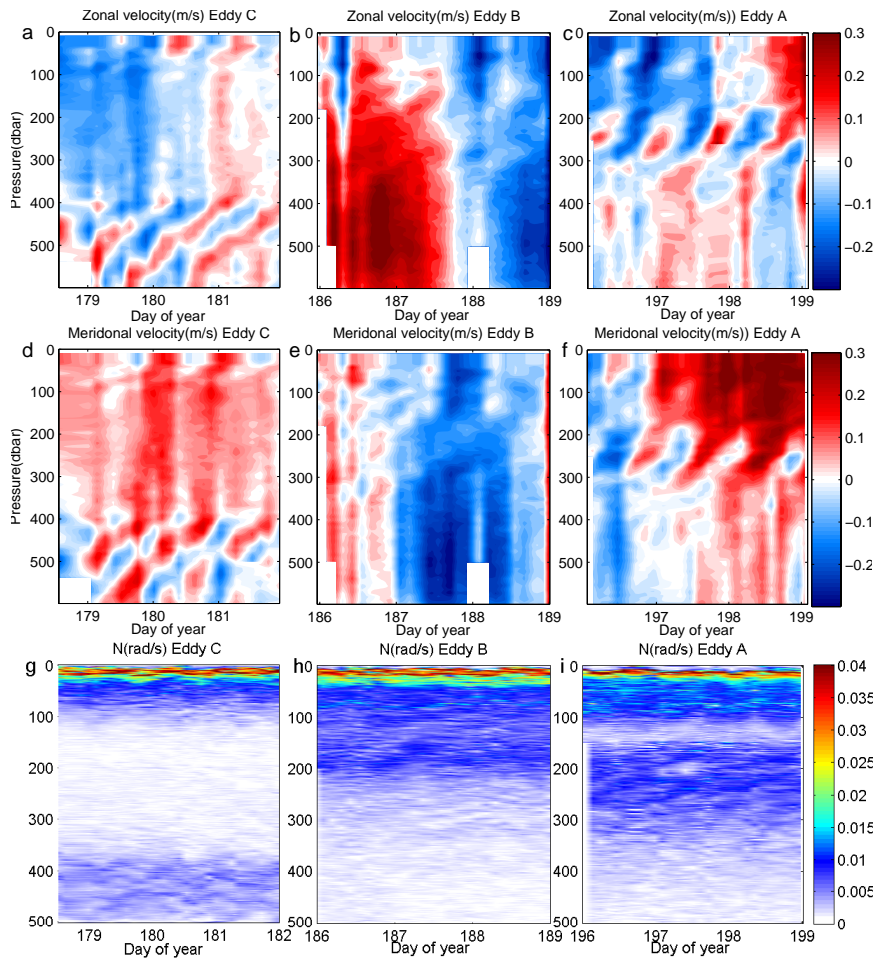
Fig. 3. Time depth plots of: **(a)**, **(b)**, **(c)** zonal velocity, **(d)**, **(e)**, **(f)** meridional velocity, **(g)**, **(h)**, **(i)** stratification profiles $N(z)$ for each LD station.

Printer-friendly Version

Interactive Discussion
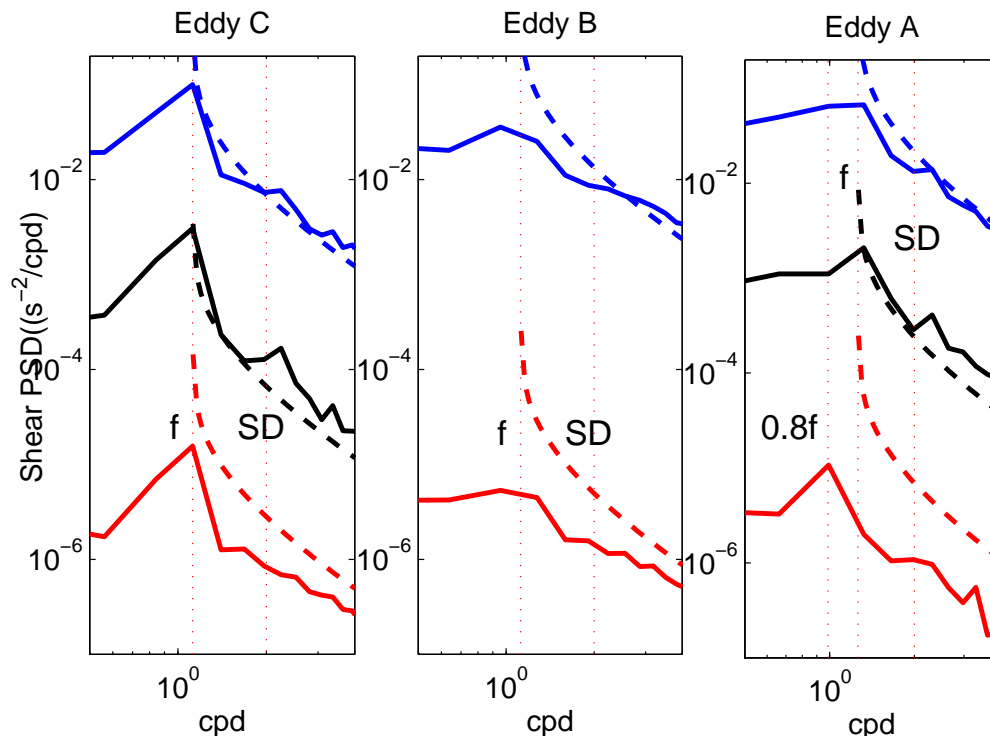
Fig. 4. Frequency spectra of LADCP vertical shear for the three eddies averaged over different depth intervals, in blue [30–500] m, in red [30–100] m, in black [400–500] m for eddy C and [200–300] m for eddy A. A two decades shift was applied between each curve. The reference spectrum, the GM model, is displayed as well for comparison in dashed lines. Vertical dashed lines mark the near inertial frequency (f) and Semi-Diurnal (SD) tide frequency.
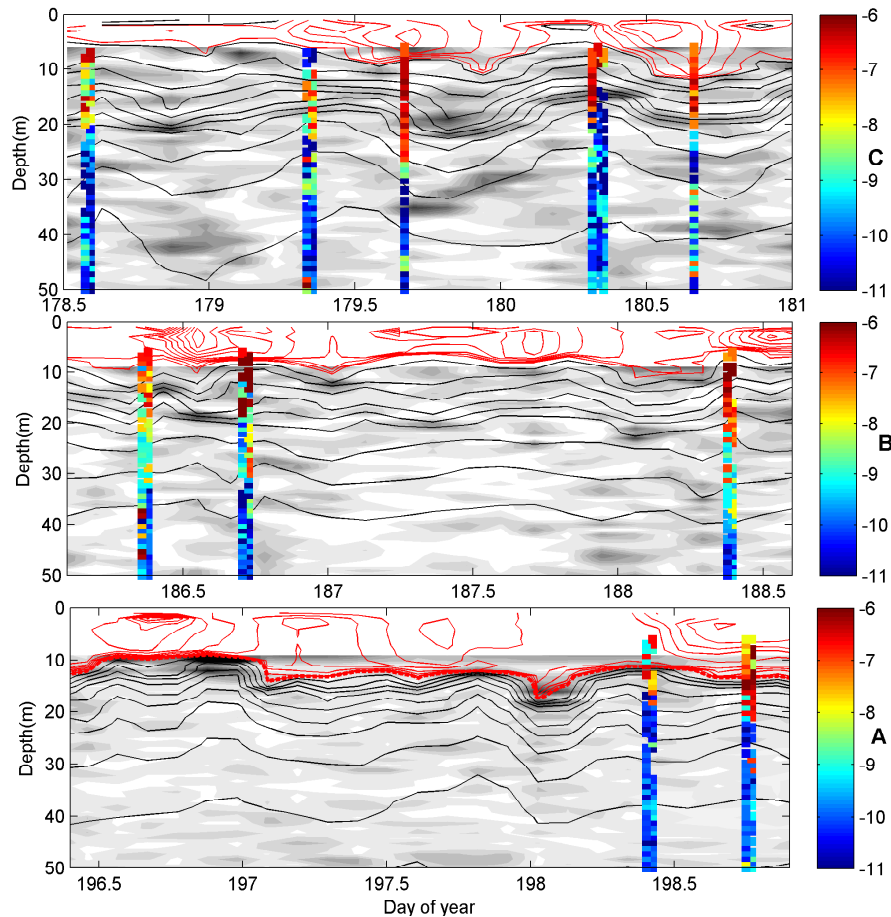
Fig. 5. Strain in gay scale, $0.03\,\mathrm{kg\,m^{-3}}$ iso-density contours in the mixed layer in red lines, $0.2\,\mathrm{kg\,m^{-3}}$ iso-density contours below the mixed layer in black and dissipation profiles in Log10 $(\mathrm{W\,kg^{-1}})$ in colored square marks, station C upper panel, station B middle panel, station A lower panel.

Title Page

Abstract | Introduction

Conclusions | References

Tables | Figures

|◄ | ►|

◄ | ►

Back | Close

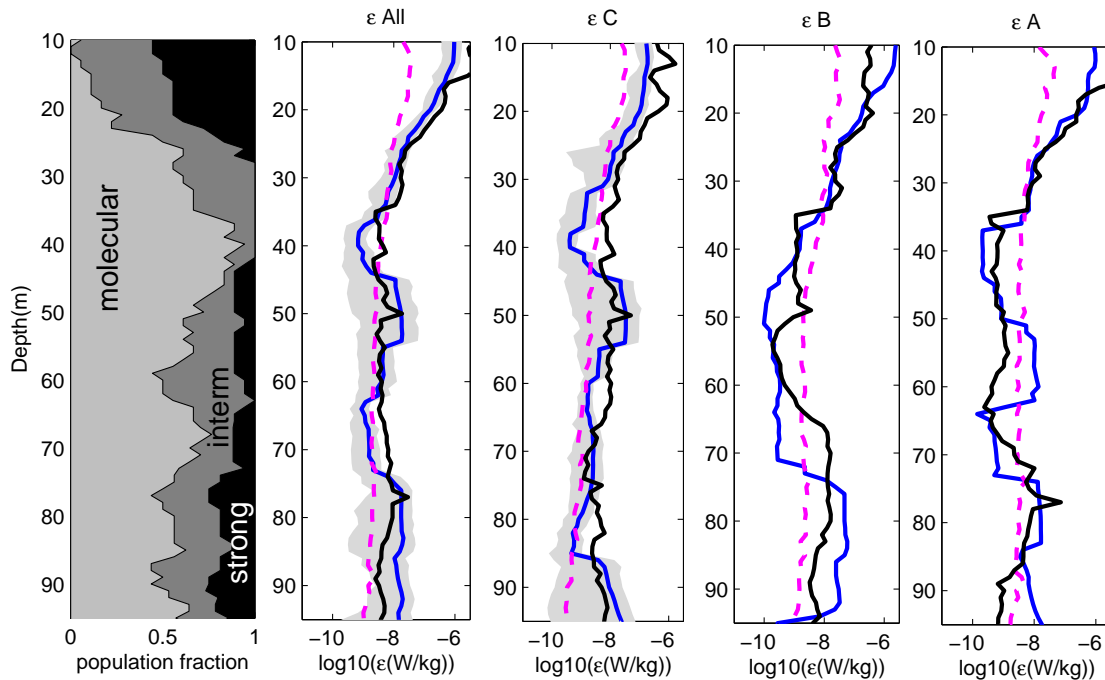Full Screen / Esc

Printer-friendly Version

Interactive Discussion
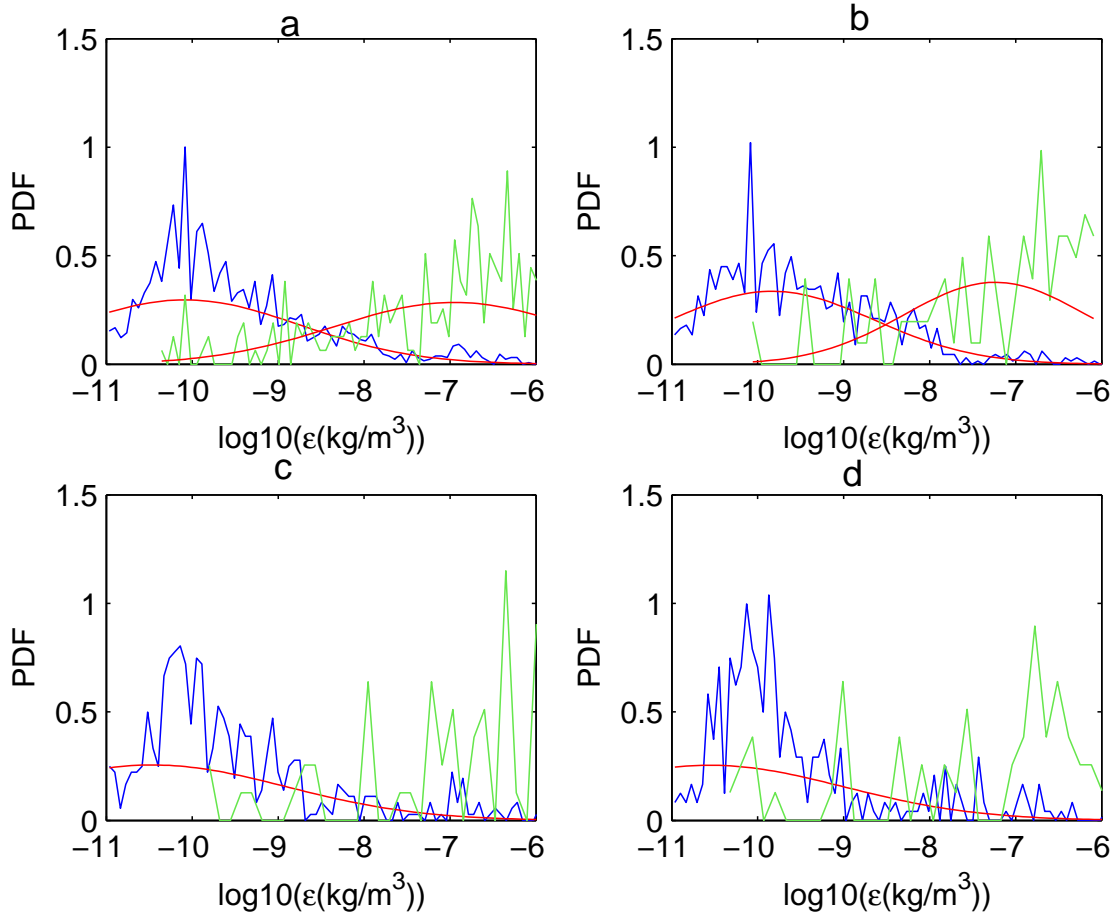
Fig. 6. Experimental PDF of $\mathrm{Log}_{10}(\varepsilon(\mathrm{W\,kg.}^{-1}))$ in grenn for $10\,\mathrm{m} < z < 20\,\mathrm{m}$ in blue for $20\,\mathrm{m} < z < 100\,\mathrm{m}$, in red MLE fit of a lognormal PDF.

Title Page

Abstract | Introduction

Conclusions | References

Tables | Figures

|◄ | ►|

◄ | ►

Back | Close

Full Screen / Esc

Printer-friendly Version

Interactive Discussion

Fig. 7. Experimental PDF of $\mathrm{Log}_{10}(K_z(\mathrm{m^2\,s.^{-1}}))$ in blue for $10\,\mathrm{m} < z < 20\,\mathrm{m}$ in blue for $20\,\mathrm{m} < z < 100\,\mathrm{m}$ in red MLE fit of a lognormal PDF.

Title Page

Abstract | Introduction

Conclusions | References

Tables | Figures

|◀ | ▶|

◀ | ▶

Back | Close

Full Screen / Esc

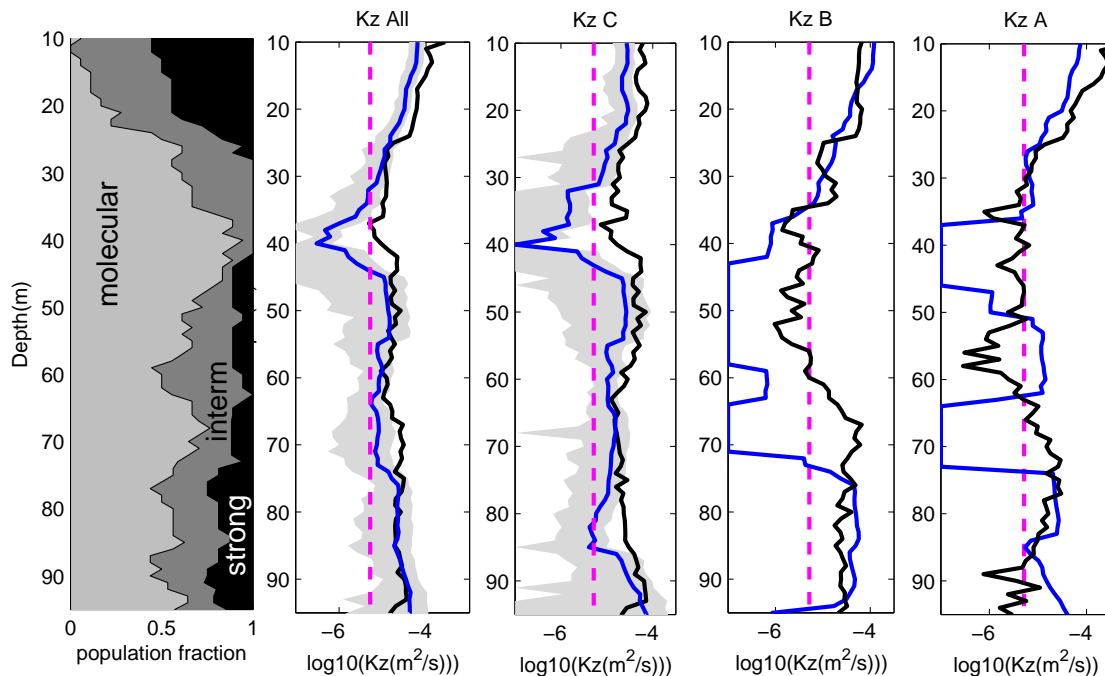Printer-friendly Version

Interactive Discussion

Fig. 8. Panel 1 proportion of the various diffusion regimes (strong, intermediate, molecular) found from SCAMP dissipation measurements. Panel 2, 3, 4, 5 overall and station averaged profiles of dissipation from SCAMP in blue plain line with 95 % confidence interval in gray shading, parameterization in black, and reference GM level in magenta dashed lines.

Fig. 9. Panel 1 proportion of the various diffusion regimes (strong, intermediate, molecular) found from SCAMP dissipation measurements. Panel 2, 3, 4, 5 overall and station averaged profiles of K_z from SCAMP in blue plain line with 95 % confidence interval in gray shading, parameterization in black, and reference GM level in magenta dashed lines.
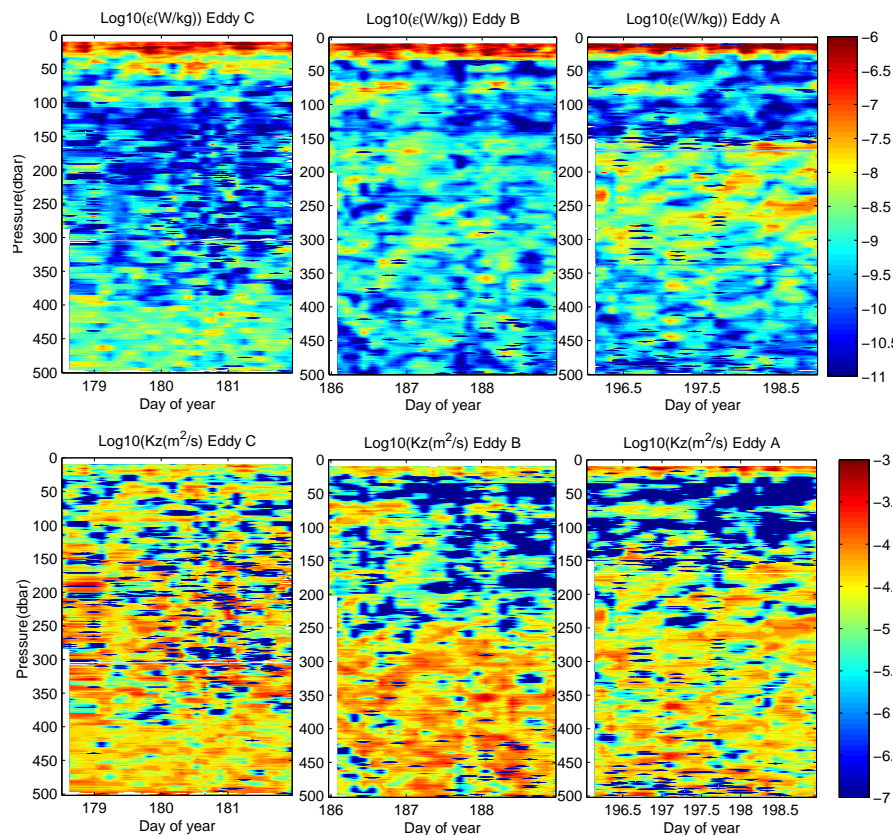
Fig. 10. Parameterized energy dissipation **(a)** and diapycnal diffusion coefficient **(b)** as a function of time and depth for the three stations.

Title Page

Abstract | Introduction

Conclusions | References

Tables | Figures

◄ | ►►

◄ | ►

Back | Close

Full Screen / Esc

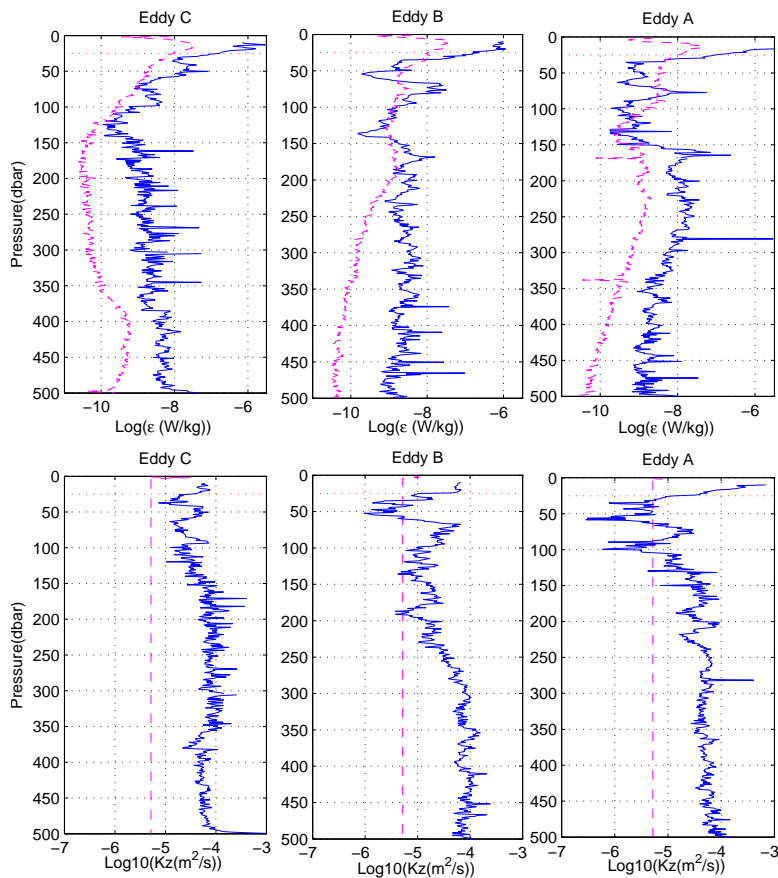Printer-friendly Version

Interactive Discussion

Fig. 11. First row: arithmetic mean (blue) and GM profiles (dashed magenta) of ϵ for the three LD stations. Second row same for K_z.
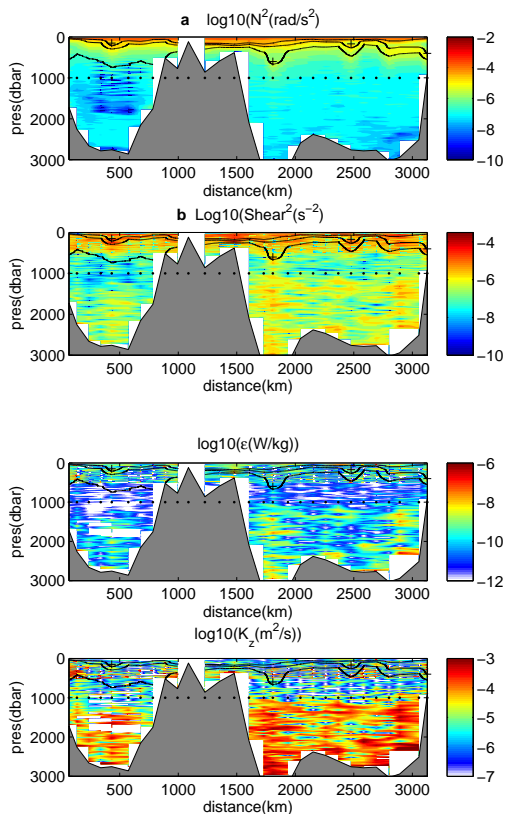
Fig. 12. Buoyancy frequency squared (N^2) **(a)**, shear squared **(b)**, dissipation rate **(c)** and diapycnal diffusivity **(d)** along the BOUM transect. The abscissae x is expressed as the distance along the transect from the fist station in the Rhone river mouth (not represented). SD stations position are marked by dots, black cross indicate approximate positions of the base of eddy A, B, C and Ierapetra eddy. Black lines represent isopycne 28.5 28.9 29.1 kg m^{-3}.

Title Page

Abstract | Introduction

Conclusions | References

Tables | Figures

◄ | ►

◄ | ►

Back | Close

Full Screen / Esc

Printer-friendly Version

Interactive Discussion